Journal of Volcanology and Geothermal Research 442 (2023) 107890

Contents lists available at ScienceDirect

Journal of Volcanology and Geothermal Research

journal homepage: www.journals.elsevier.com/journal-of-volcanology-and-geothermal-research

Decades of subsidence followed by rapid uplift: Insights from microgravity data at Askja Volcano, Iceland

M.R. Koymans [a,b,*], E. de Zeeuw-van Dalfsen [a,c], J. Sepúlveda [d], L.G. Evers [a,b], J.M. Giniaux [d], R. Grapenthin [e], A. Hooper [d], B.G. Ófeigsson [f,g], F. Sigmundsson [g], Y. Yang [g]

[a] Department of Seismology and Acoustics, Royal Netherlands Meteorological Institute, Utrechtseweg 297, De Bilt 3731 GA, Utrecht, the Netherlands
[b] Geoscience and Engineering, Delft University of Technology, Stevinweg 1, Delft 2628 CN, Zuid-Holland, the Netherlands
[c] Geoscience and Remote Sensing, Delft University of Technology, Stevinweg 1, Delft 2628 CN, Zuid-Holland, the Netherlands
[d] COMET School of Earth and Environment, University of Leeds, Woodhouse Lane, Leeds LS29JT, West Yorkshire, United Kingdom
[e] University of Alaska Fairbanks, Geophysical Institute, 2156 Koyukuk Drive, Fairbanks 9775, AK, United States
[f] Icelandic Meteorological Office, Bústaavegur 9, Reykjavík, 150, Iceland
[g] Nordic Volcanological Center, Institute of Earth Sciences, University of Iceland, Sturlugata 7 - Askja, Reykjavík 101, Iceland

ARTICLE INFO

Keywords:
Campaign
Microgravity
Data
Askja
Deformation
Volcano

ABSTRACT

In August 2021, Askja volcano in Iceland returned to the spotlight after a sudden onset of rapid uplift followed decades of continuous subsidence. In this study the extended record of microgravity data from Askja between 1988 to 2017 is revisited, and new microgravity data from 2021 and 2022 are introduced, which were collected after the uplift had started. Askja caldera had been steadily subsiding since at least 1984 and was characterised by a net decrease in microgravity, potentially signalling the contraction of its magma chamber or eviction of magma either laterally or to deeper levels. The microgravity data indicate that despite ongoing subsidence between 2017 and early 2021, a significant gravity increase can be detected in the center of the caldera between 2017 and August 2021. This increase may be introduced during – or leading up to – the period of uplift. The new microgravity data also indicate that during the period of 40 cm uplift after August 2021 to fall 2022, gravity changes approach the free-air gradient, suggesting subsurface density decreases as a driving process. This process may relate to the vesiculation of magma previously emplaced in the volcano roots, a change in the hydrothermal system, or replacement of dense basaltic magma with less dense rhyolitic magma, or a combination of these processes. However, uncertainties for this period are elevated and may obscure a gravity signal expected from additional mass accumulation. The timing and high uncertainties of some campaigns make it challenging to be conclusive on the driving process behind the uplift, but future microgravity campaigns could help solve the ambiguity. The study also provides a description of potential pitfalls in microgravity campaigns and recommendations on how the reliability of microgravity data can be improved.

1. Introduction

Long-term geodetic monitoring requires dedication. Worldwide, only a handful of volcanoes (e.g., Campi Flegrei (Berrino, 1994; Gottsmann et al., 2003), Kīlauea (Johnson et al., 2010; Bagnardi et al., 2014; Koymans et al., 2022), and Krafla (Rymer et al., 1998)) have such a uniquely extensive deformation and microgravity record as Askja, Iceland. The remarkable geodetic record of Askja enables the study of the temporal evolution of the volcano, and covers a sudden reversal in August 2021 from a four decade-long interval of subsidence of more than 1 m, that changed to rapid uplift at a rate of up to 40 cm per year. It presents an opportunity to study the geodetic signatures and to identify the source that is responsible for the observed change, and is key for hazard implications. In this pursuit, microgravity observations are beneficial because it is the only technique that can identify any potential change in subsurface mass below the caldera. One key objective of microgravity surveys in volcano monitoring is thus to detect gravimetric signatures that may indicate, or represent precursors to major changes in the character of volcanic activity that would otherwise remain undetected (e.g., Rymer (1994), Battaglia et al. (2008), Poland et al. (2021)).

* Corresponding author at: Department of Seismology and Acoustics, Royal Netherlands Meteorological Institute, Utrechtseweg 297, De Bilt 3731 GA, Utrecht, the Netherlands.
E-mail address: koymans@knmi.nl (M.R. Koymans).

https://doi.org/10.1016/j.jvolgeores.2023.107890
Received 6 May 2023; Received in revised form 7 August 2023; Accepted 12 August 2023
Available online 22 August 2023

Askja is located in the desolate highlands of central Iceland and lies at the heart of the Northern Volcanic Zone (NVZ), at the divergent boundary between the Eurasian and North American plates (Fig. 1). Near Askja, the NVZ is oriented north–south and extends in length over more than 150 km, and is locally up to 10 to 15 km wide (Sigvaldason, 1979). The divergent plate boundary hosts multiple active volcanic systems, including Askja, Bárdarbunga, Grimsvötn, and Krafla that accommodate the strain produced by the plate spreading (Drouin et al., 2017). Askja consists of nested calderas, where the main caldera has a diameter of 7 to 8 km (labeled Askja; Fig. 1), and potentially formed as the result of a Plinian eruption during the early Holocene. Alternatively, the rim of the main caldera may have been built up through sub-glacial fissure eruptions (Brown et al., 1991), accompanied by gradual caldera collapse (Gudmundsson et al., 2016). The smallest and youngest caldera (labeled Öskjuvatn; Fig. 1) developed as the result of an explosive eruption in 1875 (Sigvaldason, 1979; Sparks et al., 1981; Hartley and Thordarson, 2012). This caldera presently hosts one of the deepest lakes in Iceland. The most recent eruption at Askja was effusive and dates back to 1961 (Thorarinsson and Sigvaldason, 1962). During this eruption, basaltic lava flowed through the Öskjuop pass in the northeast of the caldera onto the flanks of the volcano, creating a convenient path into the caldera. Askja demonstrates an intermediate level of seismicity that is associated with hydrothermal activity (Greenfield et al., 2020; Winder, 2021). Hydrothermal activity is extensive and partly focused on caldera rims, but also identified surrounding lake Öskjuvatn (Ranta et al., 2023), and in the lukewarm muddy waters of Víti.

1.1. Geodetic monitoring at Askja

After the 1961 effusive eruption, a monitoring network was designed, targeted to capture the volcano's temporal evolution with a diverse set of geodetic tools (Fig. 2). Precise levelling data from a 1.7 km line are available from 1966 to 1972 (Tryggvason, 1989), and the line has been measured annually since 1983 (Sturkell and Sigmundsson, 2000; Sturkell et al., 2006; de Zeeuw-van Dalfsen et al., 2013). In the 1990s, campaign (since 1993) and continuous (since 2000) Global Navigation Satellite System (GNSS) measurements were started, and Interferometric Synthetic-Aperture Radar (InSAR) observations (since 1992) began to be included in volcano geodesy.

1.2. Subsurface structure and evolution of Askja

Leveling data indicate uplift of Askja caldera between 1970 and 1973 (Tryggvason, 1989; Sturkell et al., 2006), followed by an extended 40 year period of slowly decaying subsidence since at least 1984, and potentially as far back as 1974 when interpolated between measurements (Sturkell et al., 2006). The character of this subsidence was that of stable exponential decay with an estimated relaxation time of 39 – 42 years (Sturkell et al., 2006; Giniaux et al., 2019), and an inferred total subsidence in the center caldera of over 1 m. Deformation data from decades of subsidence indicate that a shallow magma body is likely located at approximately 2 to 3 km depth (Pagli et al., 2006; Sturkell et al., 2006; de Zeeuw-van Dalfsen et al., 2013). Nearly all modeled geodetic sources indicate a deflating point pressure source (Mogi, 1958) at approximately this depth below the center of the main caldera (Tryggvason, 1989; Rymer and Tryggvason, 1993; Sturkell and Sigmundsson, 2000; de Zeeuw-van Dalfsen et al., 2012; Drouin et al., 2017). An elliptical source model (Pagli et al., 2006), and two distinctive Mogi sources (Sturkell et al., 2006) – at depths of 3 km and 16 km, respectively – have been proposed as alternatives. Seismic tomography reveals features that represent a shallow magma storage area at 5 to 6 km depth b.s.l., and the potential existence of a magma mush storage and transport zone at 10 to 25 km depth (Mitchell et al., 2013). These models do not have sufficient resolution at 2 to 3 km and thus do not rule out the potential presence of magma at shallow depths. However, a shallow (≲3 km b.s.l.) high seismic velocity zone below the caldera may indicate an intrusive complex, with an observed low V_p/V_s ratio also suggesting the phase transition from water to steam at this depth

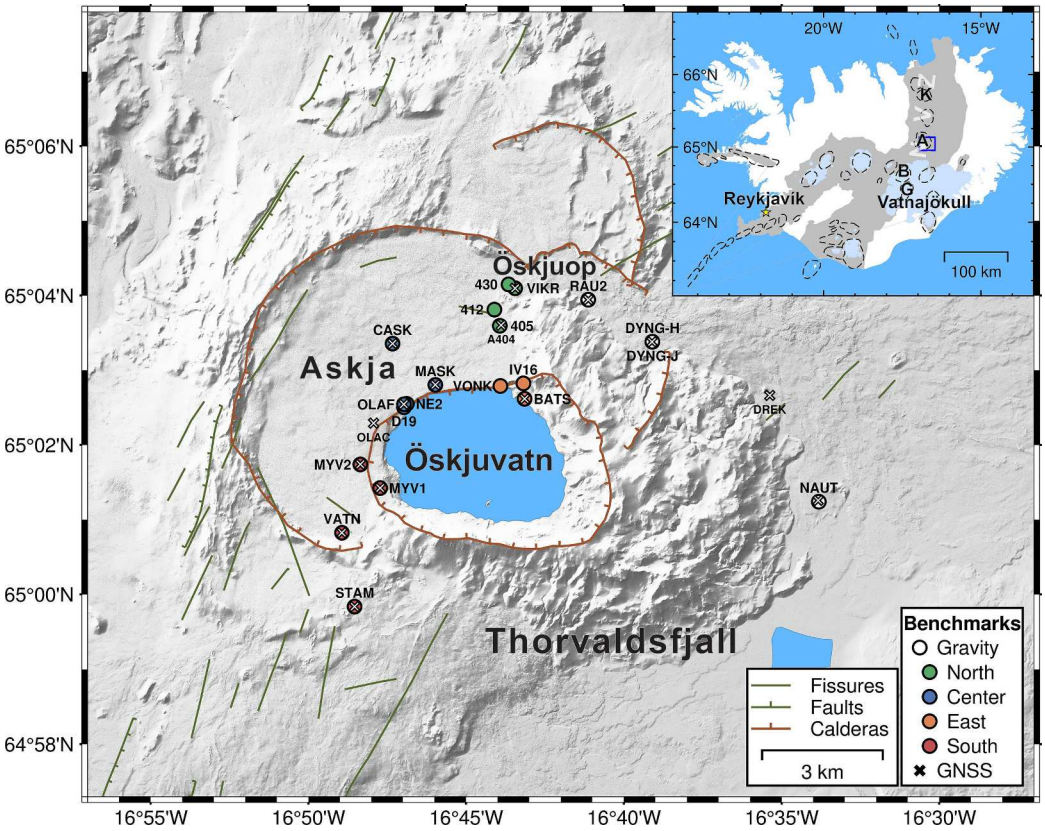

Fig. 1. Hillshaded digital elevation model of Askja highlighting the location of the caldera rims in brown (Hartley and Thordarson, 2012). The map inset shows the location of Askja and illustrates glaciers (light blue) and Icelandic volcanic zones (grey). The Northern Volcanic Zone (NVZ) stretches from the north of Krafla (K) to Askja (A) and towards Bárarbunga (B) and Grímsvötn (G). The microgravity network at Askja consists of 20 microgravity benchmarks with their identifiers. The colors represent different regional groups of microgravity benchmarks. The crosses indicate locations with continuous GNSS receivers or campaign benchmarks.

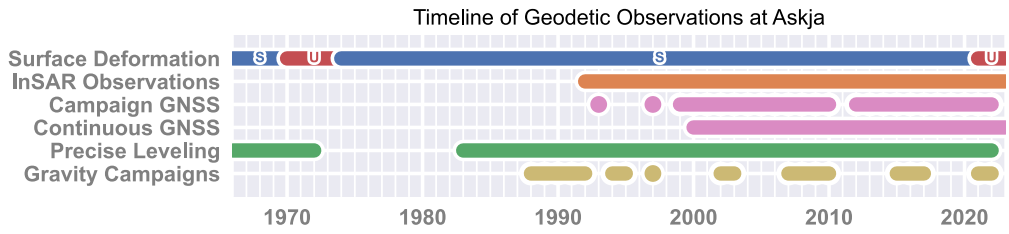

Fig. 2. Approximate coverage of geodetic monitoring techniques during periods of uplift and subsidence (U – Uplift, S – Subsidence). A continuous bar for campaign measurements indicates that data are available at least once per year. See Table 1 for the precise microgravity campaign dates and Fig. 3 for the available campaign GNSS data since 2012.

(Greenfield et al., 2016; Halldórsdóttir et al., 2010).

In August 2021, the decades-long trend of subsidence reversed, and the center caldera floor began to rise at a rate of up to 40 cm per year. The present rate of uplift identified from leveling observations indicate similar rates that were derived from leveling observations between 1971 – 1973 (Sturkell et al., 2006).

Seismic tomography and deformation modeling provides insight into source volumes, or their changes and locations, but cannot exclusively determine which mechanism is responsible for the observed surface deformation of the caldera. Microgravity surveys add information on subsurface mass changes to bridge this observational gap, and together with surface deformation data can better constrain the governing volcanic processes. Microgravity observations were started at Askja in 1988 and completed episodically in the following decades up until 2022, providing a total of 19 microgravity surveys (Table 1). For the extended period of subsidence, different source mechanisms have been suggested, such as a cooling and contracting magma chamber, and the flow from a shallow magma body to deeper levels, or through lateral movement (de Zeeuw-van Dalfsen et al., 2005). The stage of uplift that started during August 2021 has not yet been thoroughly studied and its cause remains enigmatic, but the inflection point from subsidence to uplift has been captured by geodetic observations.

In this study the full microgravity record of Askja is evaluated, joining new and previously published data. In the following sections the existing historical microgravity observations between 1988 – 2010 are reviewed, data from 2015 – 2017 are re-analysed based on available raw data, and two new microgravity campaigns from 2021 and 2022 are presented. The scope of this work focuses on the period since 1988 leading up to inflection point from extended subsidence to uplift. Microgravimetric signatures associated with the observed long-term trends in deformation are studied to investigate subsurface changes that may otherwise have remained undetected, and shed light on the governing magmatic and hydrothermal processes at Askja.

2. Methodology

2.1. Microgravity campaigns at Askja

Over the past three decades, microgravity campaigns were completed by various institutes and operators using state of the art equipment of their time (Table 1). Microgravity results between 1988 – 1991 were collected by Rymer and Tryggvason (1993) using two LaCoste & Romberg (L&R) model G instruments. Additional surveys were completed between 1992 and 2003, using similar L&R model G gravimeters, extending the established record (de Zeeuw-van Dalfsen et al., 2005). These authors also improved previously estimated net gravity changes between 1988 – 1991, with the latest two-point Mogi source model at the time to correct for height changes (Sturkell et al., 2006). Between 2007 – 2009, microgravity data were collected by Rymer et al. (2010), including another campaign completed in 2010 (de Zeeuw-van Dalfsen et al., 2013). Campaigns were restarted by Giniaux et al. (2019), who added three surveys between 2015 – 2017 using a Scintrex CG-5 gravimeter. Microgravity data were also collected in September 2021 and August 2022 in response to the observed uplift at Askja. These surveys were completed using two pairs of Scintrex CG-5, and a Scintrex CG-5 and CG-6, respectively.

Table 1
Microgravity campaigns at Askja, Iceland between 1988 – 2022. [1] Rymer and Tryggvason (1993), [2] De Zeeuw-van Dalfsen et al. (2005), [3] Rymer et al. (2013), [4] De Zeeuw-van Dalfsen et al. (2013), [5] Giniaux (2019), [6] this study. The Mogi source model for the vertical deformation correction in the 1988 – 2010 campaigns was published by Sturkell et al. (2006).

Campaign	Instruments and Serial Numbers	Deformation Correction	References
1988	L&R model G (513 and 105)	Mogi source model	[1, 2, 4]
1989	L&R model G (513 and 105)	Mogi source model	[1, 2, 4]
1990	L&R model G (513 and 105)	Mogi source model	[1, 2, 4]
1991	L&R model G (513 and 105)	Mogi source model	[1, 2, 4]
1992	L&R model G (513)	Mogi source model	[2, 4]
1994	L&R model G (513)	Mogi source model	[2, 4]
1995	L&R model G (513)	Mogi source model	[2, 4]
1997	L&R model G (513 and 403)	Mogi source model	[2, 4]
2002	L&R model G (513 and 403)	Mogi source model	[2, 4]
2003	L&R model G (513 and 403)	Mogi source model	[2, 4]
2007	L&R model G (513)	Mogi source model	[3, 4]
2008	L&R model G (513)	Mogi source model	[3, 4]
2009	L&R model G (513)	Mogi source model	[3, 4]
2010	L&R model G (513)	Mogi source model	[4]
2015	Scintrex CG-5 (968)	GNSS Measurements	[5]
2016	Scintrex CG-5 (968)	GNSS Measurements	[5]
2017	Scintrex CG-5 (968)	GNSS Measurements	[5]
2021	Scintrex CG-5 (41301) and CG-5 (41421)	GNSS Measurements	[6]
2022	Scintrex CG-5 (41301) and CG-6 (19090203)	GNSS Measurements	[6]

2.2. Askja microgravity network

The microgravity network at Askja has evolved over the past decades and consists of twenty benchmarks (Fig. 1). The network of benchmarks was initially designed and set up by Rymer and Tryggvason (1993), extended by de Zeeuw-van Dalfsen et al. (2005) in 2002 with the addition of NE2, MASK, 430, and DYNG-H, and further developed by Giniaux et al. (2019) in 2015 through the introduction of benchmarks CASK, DYNG-J, MYV1, MYV2, STAM, and VATN to improve the spatial coverage particularly in the south of the caldera. The highest density of benchmarks (MASK, OLAF, D19, and NE2) is in the center of the caldera, near the center of past subsidence and observed uplift since August 2021. After the campaign in 2022, benchmark VONK was marked for removal from the network because it is not mounted on a solid foundation and was previously measured in soil. Similarly, benchmark IV16 sits atop of a loose boulder in a region that is subject to heavy erosion and difficult to measure consistently. During the 2022 campaign, benchmark 430 appeared extremely unstable, both during the microgravity survey and the leveling measurements. Benchmark NAUT was established for future surveys at a stable point far away from the deforming caldera at an existing benchmark used for campaign GNSS measurements.

2.2.1. Microgravity network anchors

During the microgravity campaigns between 1988 and 2010, benchmark VIKR was selected as the network anchor. Beyond 2002, it was recognised that a new benchmark at DYNG, which eventually became co-located with a continuous GNSS receiver, provided a more suitable setting outside the area of active subsidence. At this site, two anchors were established: One anchor (DYNG-H) is located just beside the GNSS receiver, with the second anchor (DYNG-J) at 7 m distance. In the campaigns of 2015, 2016, and 2017, Giniaux et al. (2019) measured gravity differences relative to DYNG-J, while other campaigns in the past included an occasional measurement of DYNG-H. Both benchmarks DYNG-H and DYNG-J were measured in the 2021 and 2022 campaigns, and the effective gravity difference between the two anchors is well-constrained at a positive 170 to 180 μGal going from DYNG-H to DYNG-J. For continuity with the historical time series, all microgravity data presented in this study, including those from recent surveys (2015 – 2022) for which measurements at DYNG are available, were expressed relative to the historical anchor VIKR. Since VIKR is located in the region of deformation it may be sensitive to subsurface mass changes and net microgravity changes may be underestimated. It is recommended that the gravity network anchors are measured relative to (preferably) an absolute reference point far outside of the caldera to identify such potential problems, but logistically this may be unfeasible.

Microgravity differences between the network anchor and the benchmarks from the 1988 to 2010 campaigns were taken from the literature (Rymer and Tryggvason, 1993; de Zeeuw-van Dalfsen et al., 2005; de Zeeuw-van Dalfsen et al., 2013). Data collected by Giniaux et al. (2019) and the campaigns of 2021 and 2022 were (re-) analysed using the online tool presented in Koymans et al. (2022), simultaneously solving for instrumental drift and gravity differences (e.g., Hwang et al. (2002)), with an independent linear drift function fitted to each campaign day. Due to a limited number of measurements in the 2017 campaign, instrumental drift was fitted over the full campaign instead of daily. The microgravity data were corrected for the effect of the solid Earth tides using the default applied Scintrex tide correction (Longman, 1959). An ocean loading and polar motion correction may provide only an insignificant 1 to 2 μGal improvement to the results and was not applied.

2.3. Microgravity campaigns of 2021 and 2022

Besides reviewing and partially re-analysing the existing record of microgravity data (1988 – 2017), this study presents new data that were collected in field campaigns during September 2021 and August 2022. Both campaigns were completed with two instruments in a sub-loop (A → B → C → B → C → A), mirrored form (A → B → C → C → B → A), or a modified version thereof. Each benchmark was occupied at least twice during a campaign day, completing at minimum two sets of 5 min measurements per occupation per instrument. This strategy provides a robust dataset with a sufficient number of repeated measurements. The campaign of September 2021 is considered unreliable because it was completed in poor weather conditions, including the occasional snowstorm. In particular, high wind speeds produce high variance in the microgravity data that can be recognised in the scatter of the measurements with uncertainties of up to 20 to 30 μGal on the windiest days. The August 2022 campaign was completed in much better weather conditions and produced robust readings with an associated uncertainty on the mean gravity difference with the network anchor of 2 to 3 μGal.

2.4. Deformation correction

Corrections for relative changes in height with respect to the network anchor are made to the microgravity data. This correction is completed using the theoretical free-air gradient (FAG) of 308 μGal/m to isolate the effect of subsurface variations in mass on the microgravity observations.

Microgravity data between 1988 – 2010 are available from a series of previous publications (see Table 1). Due to the lack of GNSS coverage at this time, these data were corrected for deformation using modeled subsidence from the double Mogi point source model proposed by Sturkell et al. (2006). The change in vertical deformation between 2010 – 2015 was estimated by extrapolation from the GNSS data going back to 2012. For the campaigns between 2015 – 2022, height changes between the campaign dates were precisely estimated using co-located or measurements at nearby GNSS stations (see Fig. 1). They are all expressed relative to the vertical displacement experienced at network anchor VIKR to cancel the deformation effect at the anchor.

Continuous and campaign GNSS data in Askja from 2012 to 2022 were processed at University of Iceland using GAMIT/GLOBK 10.75 (Herring et al., 2010) together with over 100 globally distributed reference stations and continuous GNSS stations in Iceland. The solid Earth tide, ocean tide, and pole tide were corrected. The IGS final orbit products, ocean tide model FES2004 (Lyard et al., 2006), and IGS ionosphere products were applied. Only Global Positioning System (GPS) signals were used to derive the coordinates of the benchmarks. The coordinates were derived in the IGb14 reference frame aligned with ITRF2014 (Altamimi et al., 2016), and then converted to topocentric coordinate system (North, East, and Up).

3. Results

In the following sections, results from vertical deformation estimates are given, after which the net microgravity series from 1988 – 2022 expressed relative to VIKR are presented. A standardized compilation of all microgravity results from Askja since 1988, including vertical deformation estimates, can be found in tabular form in the Supplementary material (Dataset S1). In the following analysis, the microgravity benchmarks are grouped by region, following the same color scheme used in Fig. 1. The microgravity changes are not plotted on a map because there appears to be no spatial coherence outside of the regional groups, and the results lend themselves better to be presented in the form of a time series graph.

3.1. Vertical deformation estimates

The geodetic network at Askja is well designed and favorable for microgravity analysis. Since GNSS benchmarks are co-located with (or nearly adjacent to) microgravity benchmarks (Fig. 1), changes in height can be determined to within approximately 1 to 2 cm precision, equivalent to 3 to 6 μGal. In microgravity analysis, only the vertical

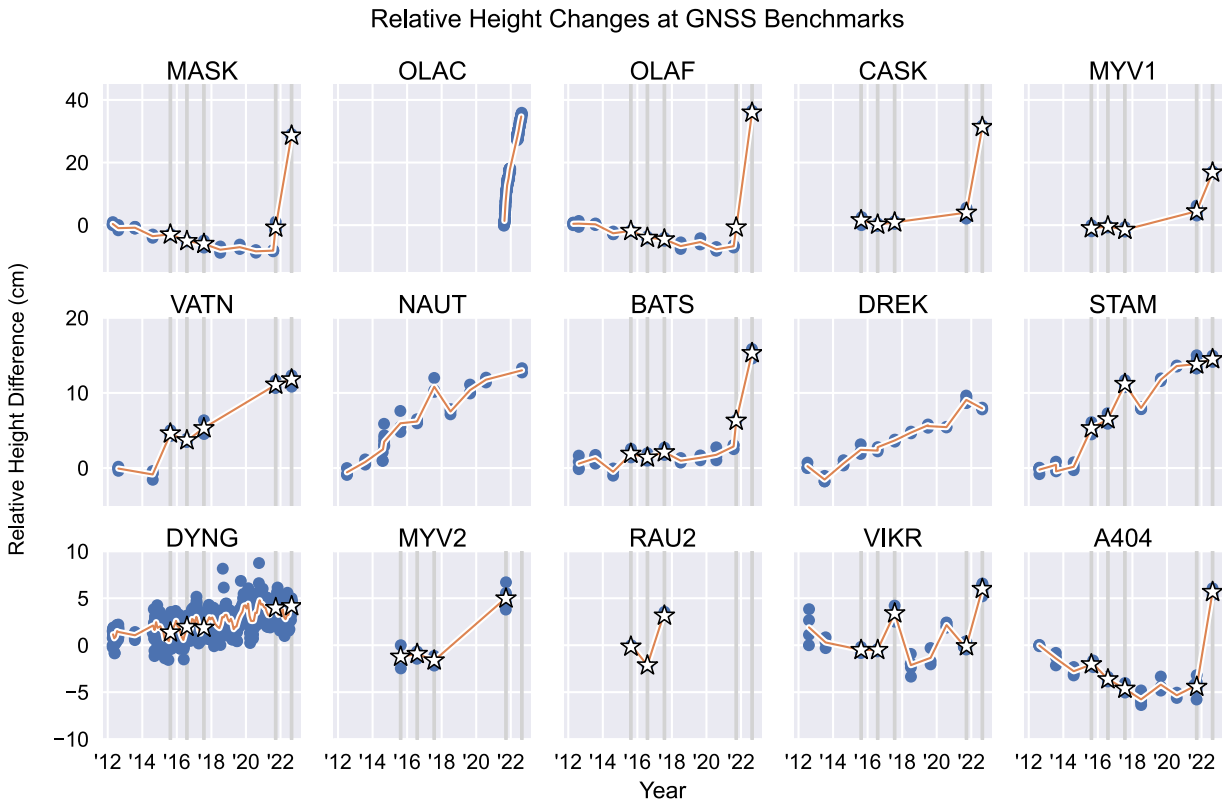

Fig. 3. Inferred vertical surface displacement (cm) between 2012–2022, expressed relative to the first measurement at each GNSS benchmark (Fig. 1). The blue dots represent campaign or continuous measurements and the orange curves interpolate between them. The vertical bars and white stars represent the selected height observations during the microgravity campaigns (Table 1) that are used for the vertical deformation correction (excluding OLAC, NAUT, and DREK). Note the different y-axis scale that is the same for all panels in each row. (For interpretation of the references to colour in this figure legend, the reader is referred to the web version of this article.)

component is considered to correct for the effect of the free-air gradient. Horizontal displacements experienced by benchmarks may be of significant amplitude, but will have no detectable effect on the microgravity measurements.

Fig. 3 illustrates the vertical surface deformation observed at various GNSS benchmarks within Askja caldera (see Fig. 1). Since 2012, GNSS benchmarks near the center of the caldera (e.g., OLAF and MASK) have been subsiding at a slow and steady rate of 1 to 2 cm per year. The reversal from subsidence to uplift of up to 40 cm per year in August 2021 can be clearly observed in benchmarks near the center of the caldera (OLAF, OLAC, MASK, and CASK). The uplift is also detected, although to a lesser extent, in the east (BATS), south (MYV1), and northern part of the caldera (A404 and VIKR). These data clearly indicate that network anchor DYNG is a more suitable network anchor than VIKR for microgravity measurements, considering the small amount of vertical deformation between campaigns that is observed at DYNG outside of seasonal variations (1 to 2 cm). However, because historical data cannot be expressed relative to anchor DYNG, benchmark VIKR, that experiences some vertical deformation during inflation, had to suffice. Regardless of this suboptimal choice, the relative changes in height between the benchmarks and VIKR is naturally accounted for.

It is noteworthy that the signal that is being recorded during the period of uplift appears to be sensed in a wider geographic area by benchmarks that were not as strongly affected by the deflationary source (e.g., BATS).

3.2. Microgravity series 1988 – 2022

Fig. 4 shows net microgravity results (corrected for the free-air gradient) since 1988, expressed relative to network anchor VIKR and the 2022 measurement. The year 2022 was selected as the base year for comparison because all benchmarks were occupied during that campaign. Microgravity changes in the center of the caldera (blue) indicate a decreasing trend relative to the first measurement in 1988, while results from the north and east region (green and orange, respectively) scatter around zero observable change. The decreasing long-term trend in the center of the caldera reaches a minimum of about − 150 to − 170 μGal towards 2016 and appears consistently in the center benchmarks. A small potential diversion from this downward trend occurred in 2007 – 2008 (40 to 60 μGal) that was recognised by Rymer et al. (2010). The possible causes that have been suggested are magma accumulation below the caldera despite continued subsidence, or changes in the hydrothermal system (de Zeeuw-van Dalfsen et al., 2013). The increase in gravity in the center benchmarks between 2016 and 2017 is challenging to verify, as the single center caldera measurement of 2016 may represent an underestimation. In 2021, a gravity increase (80 to 120 μGal) was detected relative to preceding years that cannot be accurately timed due to the extended data gap since the previous reliable campaign in 2016. During the period of uplift in 2021 and 2022, gravity did not change significantly in the center of the caldera relative to benchmark VIKR. Between 2015 – 2022 no significant changes are detected in the north and east benchmarks. It should be emphasized that these results are expressed relative to benchmark VIKR inside the caldera, which is undergoing active deformation and thus likely represent a lower bound on the gravity change estimate. Uncertainties of the historical gravity record reported in the literature are ± 20 μGal (de Zeeuw-van Dalfsen et al., 2005; de Zeeuw-van Dalfsen et al., 2013), and long-term trends should therefore be considered qualitatively.

The change from 2021 to 2022 in the center benchmarks may not be

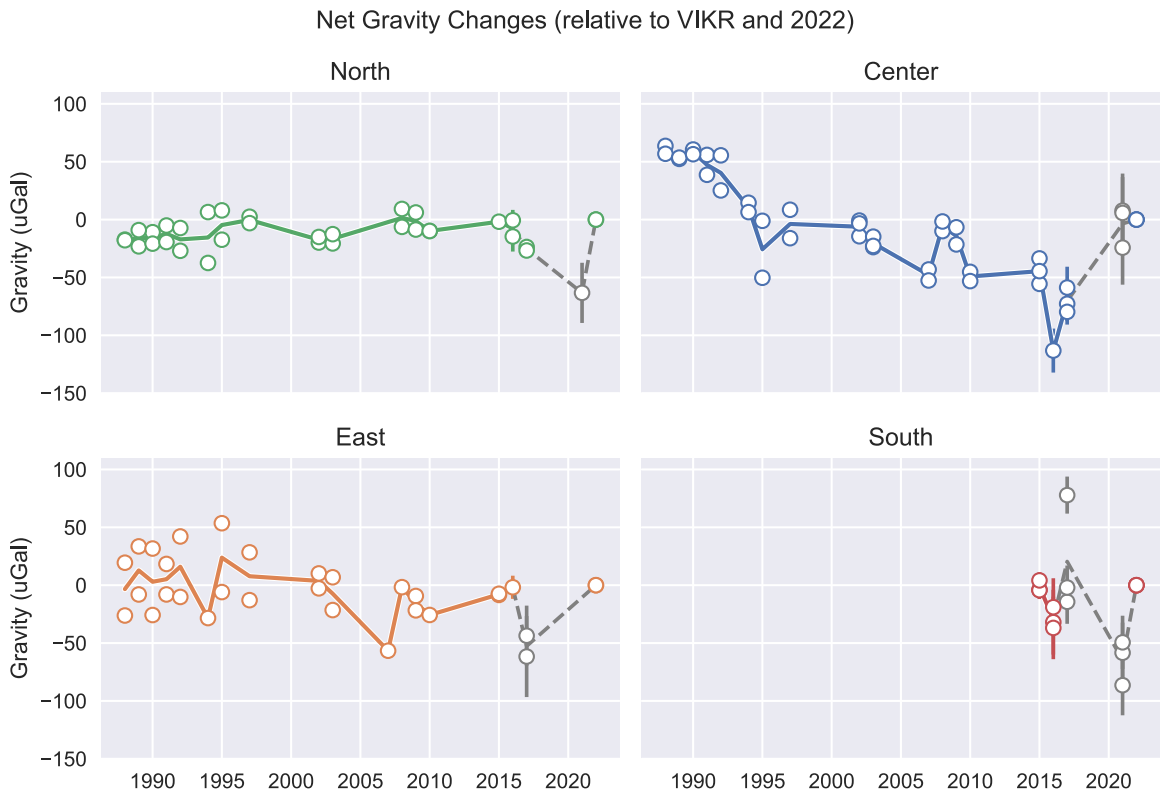

Fig. 4. Compiled net relative microgravity measurements expressed relative to anchor VIKR. Note that the data have been expressed relative to the year 2022. The colors present regional groups illustrated in Fig. 1. Microgravity changes were corrected for vertical deformation estimates using the theoretical free-air gradient of 308 μGal/m. Campaigns and groups characterised by a hybrid drift correction (2017; combining estimates of daily and full campaign instrumental drift) or large uncertainties (2021) are colored grey.

considered significant because of the poor data quality of the 2021 campaign. Uncertainties in microgravity differences for the 2015 and 2016 campaigns vary between 10 to 20 μGal. The data from the east and south group of stations in the 2017 campaign have uncertainties on the order of 40 to 75 μGal. The reason for these elevated uncertainties is that a constant linear instrumental drift had to be fit over the entire campaign to determine gravity differences for these groups. This constraint was imposed by varying circuit anchors on different days and poorly tied measurements between the anchors. Fortunately, this approach could be avoided for the center and north benchmarks because they were in a direct circuit with anchor VIKR, providing sub-20 μGal confidence limits. The uncertainty of the mean gravity differences recovered in 2021 are on the order of 10 to 30 μGal, mainly due to the strong winds. Note that the reported uncertainties represent the inferred precision of the measurements but do not provide information on the accuracy, nor the repeatability of the measurement, particularly for benchmarks that were only occupied once in a campaign. The 2022 campaign has the highest data quality with uncertainties of less than 5 μGal. In this campaign, the benchmarks nearest to the observed uplift were also measured twice during two circuits on different days. These independent measurements of the central caldera benchmarks agree to the 1 to 2 μGal level – providing the desired confidence in these results. Besides the reported precision, unquantified systemic uncertainties in microgravity results and how they can be avoided are discussed in detail below.

4. Discussion

In the following section, the sensitivity of microgravity measurements is discussed with respect to campaign strategy, user preferences in processing, and the applied deformation correction. Furthermore, the possible unknown errors that remain in the microgravity data are highlighted, along with a discussion on the repeatability of microgravity measurements. The results from the microgravity time series are then discussed in relation to the observed caldera deformation patterns.

4.1. Sensitivity of microgravity measurements

Campaign microgravity measurements are sensitive to any type of mass redistribution (Van Camp et al., 2017) and challenging to apply effectively due to their limited spatio-temporal resolution and inherently high uncertainties. The gravity effect of the level of lake Öskjuvatn, fluctuations in groundwater levels, atmospheric pressure, and snow variations cannot be accurately determined and have been neglected during the analysis, introducing an error of unknown amplitude to the microgravity results. However, all campaigns are completed in summertime when the caldera is (more or less) snow-free, limiting any potential short-period aliasing effects expected from different seasons. Besides, these effects have been shown to introduce an integrated effect that is limited to 20 μGal (Giniaux et al., 2019; Poland and de Zeeuw-van Dalfsen, 2019), within conventional demonstrated uncertainties in microgravity surveys (e.g., Rymer (1994), Battaglia et al. (2003), Gottsmann et al. (2003), Poland and de Zeeuw-van Dalfsen (2019), Koymans et al. (2022)). In addition to the uncertainty on vertical deformation measurements (1 to 2 cm), the applied gravity gradient also has an associated uncertainty. Measured free-air gradient estimates in the caldera vary between − 240 to − 360 μGal/m (Rymer and Tryggvason, 1993; de Zeeuw-van Dalfsen et al., 2005). As gradient measurements are not available for each benchmark and this value may change over time, the theoretical gradient is used for the deformation reduction

of the gravity data. Furthermore, the experienced gravity gradient also depends on the character of the source (e.g., depth). A correction using the theoretical gradient is often preferred when the source responsible for the deformation is at least a few km deep (Giniaux et al., 2019). Based on the measurements, the maximum additional error on the gravity change introduced by applying an inaccurate vertical gradient would approach − 50 to 70 μGal/m (negative means that the gravity change was overestimated).

The microgravity campaigns studied in this study were also completed with various types of instruments. The choice of instrument should in theory have no effect on the results because measurements are expressed relative to another point measured with the same instrument. Modern equipment (e.g., Scintrex CG-5, CG-6) is more convenient to operate, enabling multiple measurements in less time, assuring a more realistic drift correction. Newer gravimeters are also less prone to sudden measurement offsets (data tares). Gravimeter calibration factors may change over time (e.g., Battaglia et al. (2018)), but such an effect should in this case not influence the results significantly, because there is little variation in terrain elevation between the benchmarks at Askja, with a maximum difference of 200 m.

For the compiled microgravity record (1988 – 2022), it should be emphasized that observed gravity changes may be underestimated when they are expressed relative to network anchor VIKR located within the deforming caldera (Figs. 1 and 3). Any mass variations strong enough to be sensed at the microgravity benchmarks may potentially also be sensed at the network anchor, effectively reducing the observed relative difference and obscuring the gravity signal. Benchmark DYNG outside the caldera provides a more suitable anchor that is subject to less long-term vertical surface deformation. However, anchor VIKR is used here because it provides consistent and valuable information on the long-term gravity trend in a historical context. Future studies may consider using anchor DYNG for post-2022 surveys.

Drift corrections can be applied on a day-to-day basis (this study) as recommended by Poland and de Zeeuw-van Dalfsen (2019), or on a per-survey basis (Giniaux et al., 2019). For example, an estimate of the linear drift rate over the full survey of 2016 provides an average rate of − 470 μGal/d, while the average drift calculated over single campaign days ranges between − 1230 to 558 μGal/d. While a gravimeter operating in a lab may experience continuous monotonic drift over days, changing environments appear to impose daily variations in drift rate (Poland and de Zeeuw-van Dalfsen, 2019). Ideally, instrumental drift is estimated and corrected for on a per-circuit basis, but sometimes multi-day drift estimations cannot be avoided in the absence of anchor measurements (e.g., the 2017 campaign). For the data treated in this study, a daily drift correction is applied whenever possible, except for the 2017 campaign where a hybrid approach is employed.

Volcanic processes often produce minuscule gravimetric signatures and the choice of processing method has a demonstrable effect on the net microgravity changes. This effect may be amplified when a benchmark is only occupied once, as is the case for some measurements during the 2015 – 2017 campaigns. Single occupation measurements are particularly sensitive to variations in the assumed instrumental drift rate. This becomes especially critical when drift has to be estimated over multiple days due to e.g., the lack of consistent anchor measurements.

A campaign strategy using varying anchors between circuits can sometimes not be avoided, but it compounds the inherent uncertainty contained within the gravity measurements. It is recommended that each benchmark is measured at least twice at different times in a day, preferably in a double-loop or similar form. Multiple double measurements of benchmarks substantially help to accurately constrain the instrumental drift rate and vastly improve the confidence in the results. The adopted measurement strategy also depends on the type of instrument and for example, its susceptibility to drift, which may be lower for L&R instruments compared to modern Scintrex gravimeters. The precision and accuracy of the analysed microgravity data should be discussed. The precision of a measurement is naturally defined by its reported variance, but a second occupation with a different instrument, or on a different day, may produce a markedly different (albeit another precise) value. The measurements therefore show limited accuracy, despite the apparent high precision. This may happen for example after transport of the instrument, when insufficient time is available for the instruments to recover from tilting (Reudink et al., 2014) before the measurement is made. Repeated measurements between two CG-5 instruments in the 2021 campaign show differences of 10 to 30 μGal, and up to 80 μGal on the worst occupations. Only for the data collected during the 2022 campaign, repeated measurements at benchmarks are usually consistent to within the reported measurement precision (sub-5 μGal for the CG-6 and sub-10 μGal for the CG-5). With only a single available measurement, the recovered value is generally considered to be representative. However, a second measurement of each benchmark (besides the added contribution of this measurement in determination of instrumental drift) provides critical insight into measurement repeatability. For the occupations with widely different reported values, measurements from two instruments were averaged – unless there existed a clear indication that one measurement was more reliable than the other (e.g., low versus high precision).

The exhaustive list of possible complications illustrates why the application of campaign gravimetry in volcano monitoring remains nontrivial. The limited number of benchmarks in the caldera, and high uncertainties of the data make it difficult to provide a quantitative analysis of the recovered microgravity results. However, the results that are presented in Figs. 4 clearly indicate a long-term trend in the caldera center despite the observed yearly scatter, and also show that there is a definite coherency between measurements within regional groups. These results are discussed in the following sections.

4.2. *Microgravity signal during subsidence (1988–2021)*

The gravity record between 1988 – 2021 summarised in Fig. 4 is likely partially influenced by the process driving the subsidence of the caldera center (Pagli et al., 2006; Sturkell et al., 2006; de Zeeuw-van Dalfsen et al., 2013; Giniaux et al., 2019), acknowledging that e.g., hydrological changes may also have had a gravity effect. Generally over this period, a net microgravity decrease can be observed at the central benchmarks, suggesting a subsurface mass decrease. This observation is consistent with caldera subsidence as mass eviction is intuitively associated with deflating source volumes. Several source mechanisms have been suggested such as contraction of the magma chamber by cooling, and the removal of magma to lower levels (de Zeeuw-van Dalfsen et al., 2013). Indeed, seismic tomography from before 2013 (Mitchell et al., 2013) reveals a shallow (< 3 km b.s.l.) high velocity anomaly below the caldera, indicating elevated densities and potentially, a contracting magma chamber, but may also represent a core of denser magma deposited in post-glacial time (Brown et al., 1991; Mitchell et al., 2013). It is worth noting that the Bouguer survey conducted by Brown et al. (1991) is different from the analysis of temporal gravity changes explored here. The gravity decrease associated with subsidence may have ended in 2017 or continued until the uplift started in August 2021, but the precise ending cannot be determined confidently due to the lack of campaigns between 2017 – 2021.

The long-term decrease of the net microgravity was potentially interrupted in 2007 – 2008 and 2016 – 2017, when despite ongoing subsidence, an increase in net microgravity was observed in the eastern and center benchmarks. This observation was explained by a rising steam cap in the hydrothermal system, or magma inflow below the caldera (Rymer et al., 2010; de Zeeuw-van Dalfsen et al., 2013). However, these minor deviations may be considered noise in the long-term decreasing trend or represent an unidentified effect of the same process that went undetected by alternative geodetic techniques.

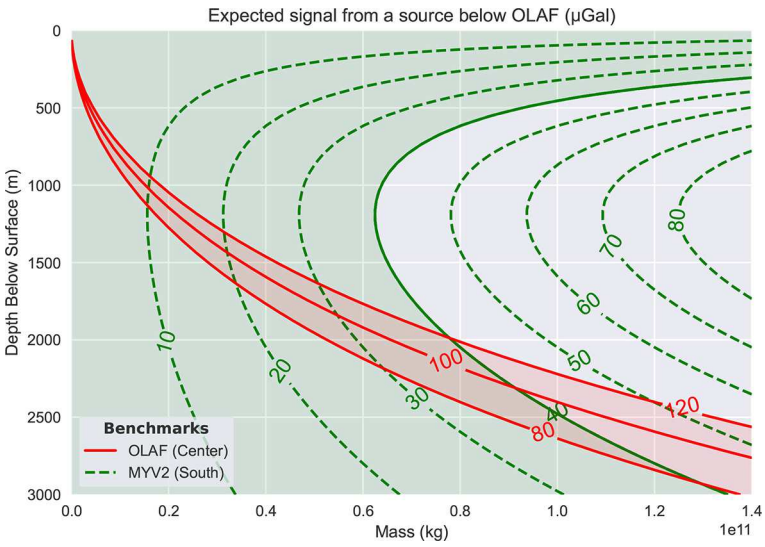

Fig. 5. Contours of the expected vertical microgravity change (μGal) for a point source at benchmark OLAF (red) and the closest non-center benchmark MYV2 (green) for a source directly below OLAF as a function of mass and depth (relative to VIKR). The solid green contour at 40 μGal represents an upper limit at which a signal would have been identified at MYV2, but was not. The intersection of the red and green areas represent the region of plausible source parameters. (For interpretation of the references to colour in this figure legend, the reader is referred to the web version of this article.)

4.3. Microgravity change leading up to and during uplift

Increases in microgravity suggest that mass has been accumulating below the center of the caldera between 2016 – 2021 in the period leading up to the uplift. This almost negated the integrated effect of the previous two decades of observed gravity decrease (Fig. 4). However, the 2021 campaign was completed while the uplift at Askja started an estimated 5 to 6 weeks earlier. The detected gravity increase of 100 μGal relative to benchmark VIKR – and potentially, a mass increase – may have played a role in causing the observed uplift. Unfortunately, the gravity increase cannot be accurately timed due to the lack of (reliable) microgravity campaigns between 2017 – 2021. This could mean that **(i)** the mass increase could have occurred right before or during the start of the uplift in August, or **(ii)** well in advance, but the magma has been filling up the available void space below the caldera first producing no detectable surface deformation, or **(iii)** the caldera does not respond elastically to the magmatic source.

The gravity change between 2017 – 2021 is only detectable in the

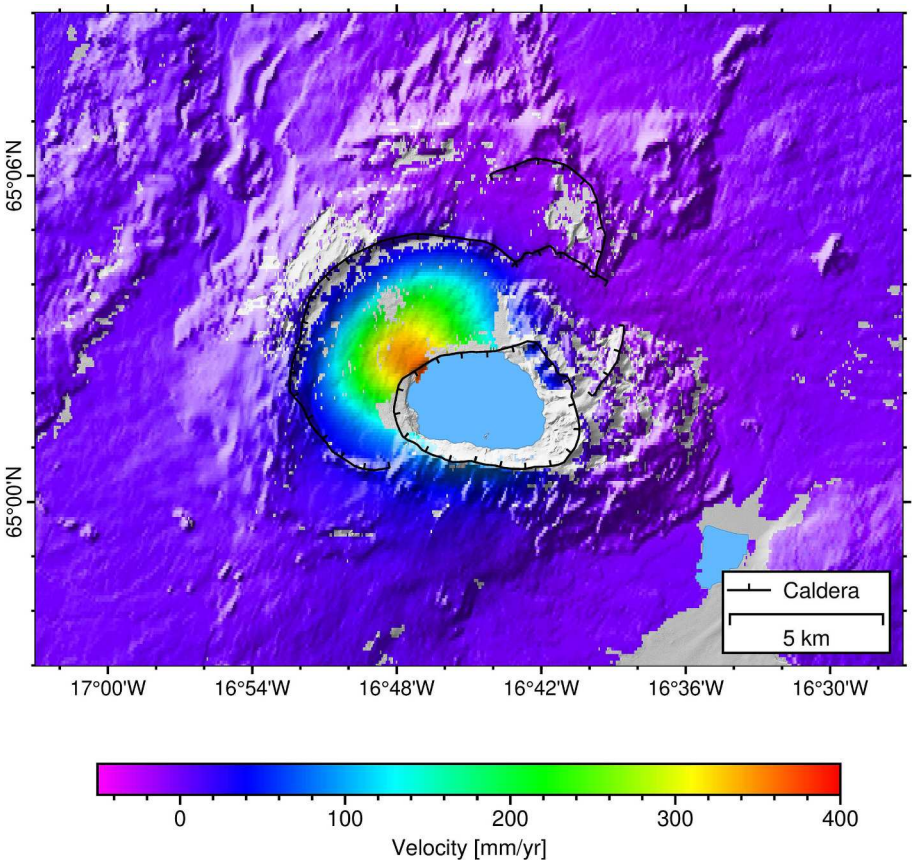

Fig. 6. InSAR deformation pattern from Askja between July 2021 and September 2022 showing the deformation rate in mm/yr. The concentric uplift pattern is clearly visible near the center of the main caldera.

group of center benchmarks (Fig. 4). This indicates that the source cannot be located at great depth with a large associated mass change. Such far-field source would have been sensed by multiple benchmarks in an broader spatial area that is not observed. However, the range of plausible source parameters for depth and mass that match the observations can be modeled (Fig. 5). Parameters of the source likely surround the 100 μGal contour of OLAF and intersect with contours falling within the uncertainty limit of the measurements at MYV2 (estimated at 40 μGal), where no signal is detected. It is therefore likely that the source is shallower than 2.5 km below the surface, and does not exceed a mass change of roughly 1×10^{11} kg.

The microgravity campaign in 2022 was completed in an attempt to capture a hypothesized microgravity increase (i.e., mass inflow) associated with the observed uplift. Since August 2021, uplift appears to be centered west and below the center caldera benchmarks (Fig. 6). However, the microgravity results show that there was no detectable increase in gravity between 2021 and 2022 after correcting for vertical deformation (Fig. 4). Despite the apparent negligible change, high uncertainties in the 2021 campaign likely obscure any deep mass variations. This observation can be considered peculiar because Askja caldera continues to experience uplift after 2021 while there appears to be no detectable change in subsurface mass. It may thus be that subsurface mass emplaced during 2016 – 2021 is responsible for the progressive uplift observed during 2022. Perhaps the accumulation of mass occurred near the end of the period of subsidence, but did not induce any apparent response on the surface. Mass inflow with a muted surface response (i.e., without deformation) may be caused by a viscoelastic response of the crust to pressurization at depth (Zurek et al., 2012), accommodated by resident gas-rich magma (Rivalta and Segall, 2008), or through the filling of voids (Johnson et al., 2010). Such a process has been detected for example at Kīlauea, Hawaii where a net microgravity increase was observed before the onset of uplift (Poland et al., 2019). Drainage of a magma body below Askja caldera between 1988 – 2016 may have created voids and cracks that could have initially been filled during 2016 – 2021 before surface deformation was detected in August 2021. The uplift after August 2021 associated with a change in gravity following the free-air gradient suggests a different process involving density decreases in the subsurface.

4.4. Insight into the driving volcanic processes

These microgravity results, when combined with the observed deformation patterns can be interpreted in terms of volcanic processes. One peculiar aspect of the recent uplift remains the limited amount of earthquakes below Askja caldera – features that are commonly associated with uplift (e.g., (Sturkell et al., 2003)) but only if the stresses experienced during subsidence are exceeded (Heimisson et al., 2015). Weak and intermediate seismicity is not unusual for Askja (Einarsson and Brandsdóttir, 2021), but during a period of significant uplift, an increase in seismicity may be expected from bulging, although that does not directly infer magma movement (Grapenthin et al., 2022). Between 2016 and 2021, no significant increase in seismicity was detected near the storage reservoirs beneath the caldera (Greenfield et al., 2020; Winder, 2021) – although seismicity associated with the ring faults surrounding the caldera increased during the period of uplift (T. Winder, personal communication). Overall, the absence of associated earthquakes may not be surprising considering that the co-eruptive and post-eruptive processes from the Holuhraun eruption in 2014 – 2015 (Pedersen et al., 2017) may have already relieved excess stress in the subsurface. Alternatively, radiating heat from an intruding source may provide a ductile regime in the subsurface that is not characterised by brittle faulting.

In summary, the gravity data indicate that Askja appears to have experienced an inflow of mass somewhere during 2016 – 2021 and is now displaying uplift through a process that introduced no further mass below the caldera (i.e., a potential density decrease). A few potential hypotheses that fit these observations are discussed and may be considered:

Firstly, simple single-source geodetic models (M. Parks, personal communication) of the recent period of uplift between 2021 – 2022 indicate an estimated volume change of 0.013 to 0.018 km^3 at 1.3 to 2.9 km depth below the surface. With a nominal magma density between 2300 to 2700 kg m^{-3} and the assumption of a point source, this would produce gravity signatures within a range of positive 20 to 90 μGal directly above the source. The lower bound of this estimate remains within the uncertainty introduced by the 2021 campaign and such intrusion may thus remain hidden within the noise. Furthermore, the transfer of magma from a deep crustal volume to another shallower volume would cause little gravity change if the volumes are spatially adjacent.

Secondly, the microgravity changes observed during uplift fall around the free-air gradient, and all gravity decreases in the raw observations can more-or-less be attributed to changes in height. Effectively, this observation indicates that a volume change is experienced, without a significant increase in subsurface mass, and hence, a density decrease may be responsible for the uplift. Processes that induce volume changes without changes in mass may be magma vesiculation (bubble-forming) through e.g., the contact of a mafic intrusion with cooler rhylotic magma (Eichelberger, 1980), second boiling of intrusions over longer time scales (Wech et al., 2020), a viscoelastic response of the crust to pressurization at depth (Zurek et al., 2012), or possibly the formation of voids (Gottsmann and Rymer, 2002; Van Camp et al., 2017). Considering the influx of mass between 2016 – 2021, the formation of voids seems unlikely, and bubbles forming from magma migrating to shallower levels may be a more suitable mechanism to explain the observations.

A third process that can produce uplift without concurrent subsurface mass accumulation would be a change in the hydrothermal system. Heat coming from the newly intruded material between 2016 and 2021 could have an effect on the extensive hydrothermal system at Askja. It is not uncommon that a process like this is expressed as significant temporal geodetic changes at volcanoes (Saibi et al., 2010). The phase transition from liquid water to steam is commonly detected at around 2 to 3 km below the surface (Greenfield et al., 2016; Halldórsdóttir et al., 2010), which may be consistent with the recovered source from surface deformation measurements. Furthermore, the center of deformation is located on the western edge of lake Öskjuvatn, around which hydrothermal activity is commonly observed (Ranta et al., 2023). Future observations of increased surface heat flow or a similar increase in the temperature of lake Öskjuvatn may support this hypothesis. Furthermore, heat from the intrusion may allow the host rock to respond in a ductile instead of brittle fashion, explaining the lack of apparent increased seismicity.

A final possibility to be considered is the replacement of denser basaltic magma ($\rho = 2800$ kg m^{-3}) with its rhyolitic ($\rho = 2400$ kg m^{-3}) counterpart. This interpretation would have implications of the hazard assessment at Askja as rhyolitic magmas are often associated with more destructive eruptions than basaltic magmas. Alternatively, it may be caused by a convecting basaltic body below the caldera where gas-rich basaltic magma is replacing denser degassed magma at shallow depth. In the case that such process is driving the uplift, surface deformation data from 2023 – 2024 will continue to show uplift with gravity changes following the free-air gradient.

The driving mechanism for the uplift remains enigmatic and further microgravity campaigns in 2023 and 2024 will help shed light on the cause of the activity. It is recommended such microgravity campaigns are completed.

5. Conclusion

Since 1988 microgravity measurements at Askja show that the extended period of subsidence coincides with an observed decrease of

around 100 to 150 μGal restricted to the center of the caldera. Microgravity differences between 2016 – 2021 indicate a significant increase (100 to 120 μGal) in gravity associated with mass accumulation in the center of the caldera occurred either during a period of subsidence before 2017, or leading up to or during the period in inflation after August 2021. Due to the lack of microgravity campaigns between 2017 – 2021, the mass increase cannot be more accurately timed. The recent period of uplift appears characterised by an insignificant change in microgravity, although a signal may still remain hidden due to the elevated uncertainty (45 μGal). Although the unambiguous interpretation of microgravity in terms of volcanic processes remains challenging, these results indicate that the surface deformation being detected in 2021 – 2022 may be a consequence of mass emplaced somewhere between 2016 and 2021. The previously emplaced mass may play a role in causing the observed uplift without the accumulation of additional mass, and likely indicates a process that involves subsurface density decreases such as magma vesiculation, a change in the hydrothermal system, the replacement of denser basaltic magma with less dense silica-rich magma, but may also represent viscoelastic or poroelastic relaxation of the subsurface.

Declaration of Competing Interest

The authors declare that they have no known competing financial interests or personal relationships that could have appeared to influence the work reported in this paper.

Data availability

Deformation data are courtesy of the University of Iceland and available via EarthScope (formerly UNAVCO). Microgravity campaign data from the 2021 and 2022 campaigns are available from 4TU (Koymans et al., 2023). Microgravity data between 2015 – 2017 were downloaded from the Leeds Data Research Repository (Giniaux, 2021). Hillshaded map data were downloaded from the National Land Survey of Iceland (2020). Geographical data include geological features (Johannesson and Sæmundsson, 2009), volcanic zones (Jakobsson et al., 2008), and glaciers (Náttúrufræistofnun Íslands – Icelandic Institute of Natural History, 2018).

Acknowledgements

Erik Sturkell, Sveinbjörn Steinórsson, and Catherine O'Hara are thanked for facilitating and joining the geodetic fieldwork at Askja. We thank Magnús T. Gudmundsson for support with the equipment. We thank the department of Geoscience & Remote Sensing of TU Delft and the University of Leeds for providing the Scintrex CG-5 and CG-6 instruments used during the 2021 and 2022 campaigns. We are grateful to one anonymous reviewer and Glyn Williams-Jones who diligently helped to improve the manuscript. Additionally, Henrietta Rákóczi is thanked for her gratuitous review of our manuscript. Figures were made with Matplotlib (Hunter, 2007), version 3.2.1 (Caswell et al., 2020). This research was supported by the EU Horizon 2020 EUROVOLC project funded by the European Commission (Grant No. 731070), the H2020 DEEPVOLC project funded by European Research Council (Grant No. 866085), and the FETOPEN-2016/2017 call (Grant No. 801221). R. G. acknowledges partial support through NSF grant EAR-1464546. COMET is the UK Natural Environment Research Council's Centre for the Observation and Modelling of Earthquakes, Volcanoes and Tectonics, a partnership between UK Universities and the British Geological Survey.

Appendix A. Supplementary data

Supplementary data associated with this article can be found, in the online version, at https://doi.org/10.1016/j.jvolgeores.2023.107890.

References

Altamimi, Z., Rebischung, P., Métivier, L., Collilieux, X., 2016. ITRF2014: a new release of the International Terrestrial Reference Frame modeling nonlinear station motions. J. Geophys. Res.: Solid Earth 121 (8), 6109–6131.

Bagnardi, M., Poland, M.P., Carbone, D., Baker, S., Battaglia, M., Amelung, F., 2014. Gravity changes and deformation at Kīlauea Volcano, Hawaii, associated with summit eruptive activity, 2009–2012. J. Geophys. Res.: Solid Earth 119 (9), 7288–7305.

Battaglia, M., Segall, P., Roberts, C., 2003. The mechanics of unrest at Long Valley caldera, California. 2. Constraining the nature of the source using geodetic and micro-gravity data. J. Volcanol. Geoth. Res. 127 (3–4), 219–245.

Battaglia, M., Gottsmann, J., Carbone, D., Fernández, J., 2008. 4D volcano gravimetry. Geophysics 73 (6), WA3–WA18.

Battaglia, M., Lisowski, M., Dzurisin, D., Poland, M.P., Schilling, S., Diefenbach, A., Wynn, J., 2018. Mass addition at Mount St. Helens, Washington, inferred from repeated gravity surveys. J. Geophys. Res.: Solid Earth 123 (2), 1856–1874.

Berrino, G., 1994. Gravity changes induced by height-mass variations at the Campi Flegrei caldera. J. Volcanol. Geoth. Res. 61 (3–4), 293–309.

Brown, G., Everett, S., Rymer, H., McGarvie, D., Foster, I., 1991. New light on caldera evolution—Askja, Iceland. Geology 19 (4), 352–355.

Caswell, T.A., Droettboom, M., Lee, A., Hunter, J., Firing, E., Stansby, D., Klymak, J., Hoffmann, T., de Andrade, E.S., Varoquaux, N., Nielsen, J.H., Root, B., Elson, P., May, R., Dale, D., Lee, J.-J., Seppänen, J.K., McDougall, D., Straw, A., Hobson, P., Gohlke, C., Yu, T.S., Ma, E., Vincent, A.F., Silvester, S., Moad, C., Kniazev, N., Ivanov, P., Ernest, E., Katins, J., 2020. matplotlib/matplotlib: REL: v3.2.1, doi: 10.5281/zenodo.3714460.

de Zeeuw-van Dalfsen, E., Rymer, H., Sigmundsson, F., Sturkell, E., 2005. Net gravity decrease at Askja volcano, Iceland: constraints on processes responsible for continuous caldera deflation, 1988–2003. J. Volcanol. Geoth. Res. 139 (3–4), 227–239.

de Zeeuw-van Dalfsen, E., Pedersen, R., Hooper, A., Sigmundsson, F., 2012. Subsidence of Askja caldera 2000–2009: Modelling of deformation processes at an extensional plate boundary, constrained by time series InSAR analysis. J. Volcanol. Geoth. Res. 213, 72–82.

de Zeeuw-van Dalfsen, E., Rymer, H., Sturkell, E., Pedersen, R., Hooper, A., Sigmundsson, F., Ófeigsson, B., 2013. Geodetic data shed light on ongoing caldera subsidence at Askja, Iceland. Bull. Volcanol. 75 (5), 1–13.

Drouin, V., Sigmundsson, F., Ófeigsson, B.G., Hreinsdóttir, S., Sturkell, E., Einarsson, P., 2017. Deformation in the Northern Volcanic Zone of Iceland 2008–2014: an interplay of tectonic, magmatic, and glacial isostatic deformation. J. Geophys. Res.: Solid Earth 122 (4), 3158–3178.

Eichelberger, J., 1980. Vesiculation of mafic magma during replenishment of silicic magma reservoirs. Nature 288 (5790), 446–450.

Einarsson, P., Brandsdóttir, B., 2021. Seismicity of the Northern Volcanic Zone of Iceland. Front. Earth Sci. 9, 628967.

Giniaux, J.M., 2019. Constraints on Askja Volcano, Iceland, from Surface Deformation and Gravity Change.

Gottsmann, J., Rymer, H., 2002. Deflation during caldera unrest: constraints on subsurface processes and hazard prediction from gravity–height data. Bull. Volcanol. 64 (5), 338–348.

Giniaux, J., 2021. Gravity campaigns at Askja Volcano (Iceland), in 2015, 2016 and 2017, using the Scintrex CG-5 968, 2021. https://doi.org/10.5518/1030.

Gottsmann, J., Berrino, G., Rymer, H., Williams-Jones, G., 2003. Hazard assessment during caldera unrest at the Campi Flegrei, Italy: a contribution from gravity–height gradients. Earth Planet. Sci. Lett. 211 (3–4), 295–309.

Grapenthin, R., Cheng, Y., Angarita, M., Tan, D., Meyer, F.J., Fee, D., Wech, A., 2022. Return from dormancy: rapid inflation and seismic unrest driven by transcrustal magma transfer at Mt. Edgecumbe (L'úx Shaa) Volcano, Alaska. Geophys. Res. Lett. 49 (20), e2022GL099464.

Greenfield, T., White, R.S., Roecker, S., 2016. The magmatic plumbing system of the Askja central volcano, Iceland, as imaged by seismic tomography. J. Geophys. Res.: Solid Earth 121 (10), 7211–7229.

Greenfield, T., White, R.S., Winder, T., Ágústsdóttir, T., 2020. Seismicity of the Askja and Bárðarbunga volcanic systems of Iceland, 2009–2015. J. Volcanol. Geoth. Res. 391, 106432.

Gudmundsson, M.T., Jónsdóttir, K., Hooper, A., Holohan, E.P., Halldórsson, S.A., Ófeigsson, B.G., Cesca, S., Vogfjörd, K.S., Sigmundsson, F., Högnadóttir, T., et al., 2016. Gradual caldera collapse at Bárdarbunga volcano, Iceland, regulated by lateral magma outflow. Science 353 (6296), aaf8988.

Halldórsdóttir, S., Björnsson, H., Mortensen, A.K., Axelsson, G., Á. Guðmundsson, 2010. Temperature model and volumetric assessment of the Krafla geothermal field in N-Iceland. In: World Geothermal Congress, 25–29, 2010.

Hartley, M., Thordarson, T., 2012. Formation of Öskjuvatn caldera at Askja, North Iceland: Mechanism of caldera collapse and implications for the lateral flow hypothesis. J. Volcanol. Geoth. Res. 227, 85–101.

Heimisson, E.R., Einarsson, P., Sigmundsson, F., Brandsdóttir, B., 2015. Kilometer-scale Kaiser effect identified in Krafla volcano, Iceland. Geophys. Res. Lett. 42 (19), 7958–7965.

Herring, T., King, R., McClusky, S., et al., 2010. Introduction to GAMIT/GLOBK, Massachusetts Institute of Technology, Cambridge, Massachusetts.

Hunter, J.D., 2007. Matplotlib: a 2D graphics environment. Comput. Sci. Eng. 9 (3), 90–95. https://doi.org/10.1109/MCSE.2007.55.

Hwang, C., Wang, C.-G., Lee, L.-H., 2002. Adjustment of relative gravity measurements using weighted and datum-free constraints. Comput. Geosci. 28 (9), 1005–1015.

Jakobsson, S.P., Jónasson, K., Sigurdsson, I.A., 2008. The three igneous rock series of Iceland. Jökull 58, 117–138.
Johannesson, H., Sæmundsson, K., 2009. Geological Map of Iceland, 1:500 000. Tectonics.
Johnson, D.J., Eggers, A.A., Bagnardi, M., Battaglia, M., Poland, M.P., Miklius, A., 2010. Shallow magma accumulation at Kīlauea Volcano, Hawai ʻi, revealed by microgravity surveys. Geology 38 (12), 1139–1142.
Koymans, M.R., de Zeeuw-van Dalfsen, E., Evers, L.G., Poland, M.P., 2022. Microgravity change during the 2008–2018 Kılauea Summit Eruption: Nearly a Decade of Subsurface Mass Accumulation. J. Geophys. Res.: Solid Earth 127 (9), e2022JB024739, doi:10.1029/2022JB024739.
Koymans, M., de Zeeuw-van Dalfsen, E., Hooper, A., Araya, J., 2023. Dataset of microgravity campaign measurements from the Askja volcano. doi:10.4121/912B666B-95C0-4F93-9485-E98256517991.V1, URL: https://data.4tu.nl/datasets/912b666b-95c0-4f93-9485-e98256517991/1.
Longman, I., 1959. Formulas for computing the tidal accelerations due to the moon and the sun. J. Geophys. Res. 64 (12), 2351–2355.
Lyard, F., Lefevre, F., Letellier, T., Francis, O., 2006. Modelling the global ocean tides: modern insights from FES2004. Ocean Dynam. 56 (5), 394–415.
Mitchell, M.A., White, R.S., Roecker, S., Greenfield, T., 2013. Tomographic image of melt storage beneath Askja Volcano, Iceland using local microseismicity. Geophys. Res. Lett. 40 (19), 5040–5046.
Mogi, K., 1958. Relations between the eruptions of various volcanoes and the deformations of the ground surfaces around them. Earthq. Res. Inst. 36, 99–134.
National Land Survey of Iceland, Iceland Hillshade Digital Elevation Model (50m), 2020.
Náttúrufræistofnun Íslands – Icelandic Institute of Natural History, NI_VG25 Vistgerir á Íslandi 2. útgáfa – 1:25.000, 2018.
Pagli, C., Sigmundsson, F., Arnadóttir, T., Einarsson, P., Sturkell, E., 2006. Deflation of the Askja volcanic system: constraints on the deformation source from combined inversion of satellite radar interferograms and GPS measurements. J. Volcanol. Geoth. Res. 152 (1–2), 97–108.
Pedersen, G., Höskuldsson, A., Dürig, T., Thordarson, T., Jonsdottir, I., Riishuus, M., Óskarsson, B., Dumont, S., Magnússon, E., Gudmundsson, M.T., et al., 2017. Lava field evolution and emplacement dynamics of the 2014–2015 basaltic fissure eruption at Holuhraun, Iceland. J. Volcanol. Geoth. Res. 340, 155–169.
Poland, M.P., de Zeeuw-van Dalfsen, E., 2019. Assessing seasonal changes in microgravity at Yellowstone caldera. J. Geophys. Res.: Solid Earth 124 (4), 4174–4188.
Poland, M.P., de Zeeuw-van Dalfsen, E., Bagnardi, M., Johanson, I.A., 2019. Post-collapse gravity increase at the summit of Kīlauea volcano, Hawaii. Geophys. Res. Lett. 46 (24), 14430–14439.
Poland, M.P., Carbone, D., Patrick, M.R., 2021. Onset and evolution of Kīlauea's 2018 flank eruption and summit collapse from continuous gravity. Earth Planet. Sci. Lett. 567, 117003.
Ranta, E., Halldórsson, S.A., Barry, P.H., Ono, S., Robin, J.G., Kleine, B.I., Ricci, A., Fiebig, J., Sveinbjörnsdóttir, Á.E., Stefánsson, A., 2023. Deep magma degassing and volatile fluxes through volcanic hydrothermal systems: Insights from the Askja and Kverkfjöll volcanoes, Iceland. J. Volcanol. Geoth. Res. 436, 107776 https://doi.org/10.1016/j.jvolgeores.2023.107776.
Reudink, R., Klees, R., Francis, O., Kusche, J., Schlesinger, R., Shabanloui, A., Sneeuw, N., Timmen, L., 2014. High tilt susceptibility of the Scintrex CG-5 relative gravimeters. J. Geodesy 88 (6), 617–622.
Rivalta, E., Segall, P., 2008. Magma compressibility and the missing source for some dike intrusions. Geophys. Res. Lett. 35 (4).
Rymer, H., 1994. Microgravity change as a precursor to volcanic activity. J. Volcanol. Geoth. Res. 61 (3–4), 311–328.
Rymer, H., Tryggvason, E., 1993. Gravity and elevation changes at Askja, Iceland. Bull. Volcanol. 55 (5), 362–371.
Rymer, H., Cassidy, J., Locke, C.A., Sigmundsson, F., 1998. Post-eruptive gravity changes from 1990 to 1996 at Krafla volcano, Iceland. J. Volcanol. Geoth. Res. 87 (1–4), 141–149.
Rymer, H., Locke, C., Ófeigsson, B.G., Einarsson, P., Sturkell, E., 2010. New mass increase beneath Askja volcano, Iceland–a precursor to renewed activity? Terra Nova 22 (4), 309–313.
Saibi, H., Gottsmann, J., Ehara, S., 2010. Post-eruptive gravity changes from 1999 to 2004 at Unzen volcano (Japan): A window into shallow aquifer and hydrothermal dynamics. J. Volcanol. Geoth. Res. 191 (1–2), 137–147.
Sigvaldason, G.E., 1979. Rifting, magmatic activity and interaction between acid and basic liquids. Nordic Volcanol. Inst., 79 (03).
Sparks, R.S.J., Wilson, L., Sigurdsson, H., 1981. The pyroclastic deposits of the 1875 eruption of Askja, Iceland. Philos. Trans. Roy. Soc. London. Ser. A, Math. Phys. Sci. 299 (1447), 241–273.
Sturkell, E., Sigmundsson, F., 2000. Continuous deflation of the Askja caldera, Iceland, during the 1983–1998 noneruptive period. J. Geophys. Res.: Solid Earth 105 (B11), 25671–25684.
Sturkell, E., Sigmundsson, F., Einarsson, P., 2003. Recent unrest and magma movements at Eyjafjallajökull and Katla volcanoes, Iceland. J. Geophys. Res.: Solid Earth 108 (B8).
Sturkell, E., Sigmundsson, F., Slunga, R., 2006. 1983–2003 decaying rate of deflation at Askja caldera: pressure decrease in an extensive magma plumbing system at a spreading plate boundary. Bull. Volcanol. 68 (7), 727–735.
Thorarinsson, S., Sigvaldason, G.E., 1962. The eruption in Askja, 1961; a preliminary report. Am. J. Sci. 260 (9), 641–651.
Tryggvason, E., 1989. Ground deformation in Askja, Iceland: its source and possible relation to flow of the mantle plume. J. Volcanol. Geotherm. Res. 39 (1), 61–71.
Van Camp, M., de Viron, O., Watlet, A., Meurers, B., Francis, O., Caudron, C., 2017. Geophysics from terrestrial time-variable gravity measurements. Rev. Geophys. 55 (4), 938–992.
Wech, A.G., Thelen, W.A., Thomas, A.M., 2020. Deep long-period earthquakes generated by second boiling beneath Mauna Kea volcano. Science 368 (6492), 775–779.
Winder, T., 2021. Tectonic earthquake swarms in the Northern Volcanic Zone, Iceland, Apollo - University of Cambridge Repository doi:10.17863/CAM.82505.
Zurek, J., William-Jones, G., Johnson, D., Eggers, A., 2012. Constraining volcanic inflation at Three Sisters Volcanic Field in Oregon, USA, through microgravity and deformation modeling. Geochem. Geophys. Geosyst. 13 (10), Q10013. https://doi.org/10.1029/2012gc004341.